

Highly photoactive ZnO by amine capping-assisted hydrothermal treatment

G. Colón^{a,*}, M.C. Hidalgo^a, J.A. Navío^a, E. Pulido Melián^b,
O. González Díaz^b, J.M. Doña Rodríguez^b

^a*Instituto de Ciencia de Materiales de Sevilla, Centro Mixto CSIC-Universidad de Sevilla, Américo Vespucio s/n, 41092, Sevilla, Spain*

^b*Centro Instrumental Químico-Físico para el Desarrollo de Investigación Aplicada (CIDIA), Departamento de Química, Universidad de Las Palmas de Gran Canaria, Edificio Central del Parque Científico Tecnológico, Campus de Tafira, 35017, Las Palmas, Spain*

Received 15 November 2007; received in revised form 16 January 2008; accepted 24 January 2008

Available online 9 February 2008

Abstract

ZnO nanoparticles have been prepared by amine template assisted sol–gel precipitation and further hydrothermal treatment. We have investigated the effect of different pH values achieved by means of triethylamine (TEA) addition in the final surface and structural properties. Two sets of samples were obtained after thermal treatment, one with no hydrothermal pre-treatment and a second hydrothermally pre-treated. Surprisingly the precipitate obtained after the amine addition also exhibits good photocatalytic properties. It has been stated that calcination treatment leads in both sets of samples to a significant improvement in the photocatalytic properties of the studied systems. Therefore, interesting comparison has been performed between hydrothermal pre-treated and direct thermal treated samples. Surface and morphological features notably differ from ZnO prepared using different synthetic route. Wide surface and structural characterization of the samples have been carried out, and correlations with precipitation pH are pointed out from this characterization. In all cases, the amine templated ZnO obtained exhibit high conversion values for phenol photo-oxidation reaction. Further calcination treatment in all of the studied samples clearly leads to photocatalytic conversions higher than that exhibited by TiO₂ Degussa P25. This fact is even more significant if we consider that hydrothermally and calcined ZnO exhibit almost null surface area values, leading to a startling intrinsic photoactivity. The structural excellence (crystallinity, lack of defects, crystallite size, etc.) of such systems is clearly responsible for their high photoactivity values.

© 2008 Elsevier B.V. All rights reserved.

Keywords: ZnO; Triethylamine; Hydrothermal; Photocatalysis

1. Introduction

It is well established that morphological and structural parameters strongly affect the photocatalytic activity of a semiconductor [1,2]. The synthesis of nanoparticles with controlled size and composition is of technological interest. As a consequence, there has been a lot of highlighting on the production of nanoparticulated semiconductors (TiO₂, ZnO, SnO₂, ...) for a wide range of applications, including photocatalysis. Within this framework, the proposal of new synthetic routes for obtaining highly photoactive nanoparticles appears extremely interesting. From the point of view of the enhancement in the efficiencies of the photocatalytic process,

it is evident that the tailoring and development of new and alternative photocatalysts can be considered of great interest. The approach to new photocatalytic systems goes through the modification in the synthetic process as well as the design of new systems and configurations (nanotubes, mesoporous, thin films, ...) [1].

Zinc oxide is a direct band-gap semiconductor with applications in a wide range of fields such as optoelectronic or photocatalysis. It is widely reported that the main properties of ZnO nanostructures strongly depends on their morphology, crystalline structure, defect and impurity contents. In this sense, the ZnO preparation route affects in a significant way to those properties. Thus, a large number of physical techniques such as magnetron sputtering [3], pulsed laser deposition [4,5], spray pyrolysis [6,7], vapour and vapour–liquid–solid growth [8], or plasma induced vapour deposition are used for obtaining nanostructured ZnO. However, there are not many efforts

* Corresponding author.

E-mail address: gcolon@icmse.csic.es (G. Colón).

regarding low temperature chemical techniques [9]. It has been demonstrated that the hydrothermal synthesis is a feasible route for the preparation of ZnO nanoparticles with controlled morphology, structure and surface area [10,11]. For photocatalytic applications, the improvement of the photoactivity might be achieved by influencing those properties that control either the charge carrier dynamics (carrier generation, transfer and diffusion) or the surface catalytic process, which are the quality of the structure and the surface features. In this sense, it is widely reported that the hydrothermal synthesis would provide the adequate structural and surface properties for photocatalytic applications [12].

In previous papers we reported a wide study of highly photoactive TiO₂ systems prepared by hydrothermal method from a Ti⁴⁺ water solution [13,14]. The correlations between the route parameters and the final surface and structural properties demonstrate the importance of controlling the synthetic steps. We concluded that hydrothermal treatment does not grant the finest performance in the catalyst for a photocatalytic application [13]. A further calcination treatment provides an optimal structural situation, and as a result, joints surface and structural contributions lead to better photoactivity rates for phenol degradation. For this purpose, we continue the study with the hydrothermal preparation of ZnO from Zn²⁺ water solution trying to optimize the synthetic route for photocatalytic applications.

2. Experimental

ZnO photocatalysts have been obtained by precipitation of 0.25 M aqueous Zn²⁺ solutions from zinc acetate and acidified by means of acetic acid. The pH of this Zn²⁺ solution was 3.6. The precipitation was achieved at pH values of 8 and 11 and by using triethylamine (TEA) as precipitating agent. Then, a certain amount of triethylamine was then added drop wise to the Zn-solution aliquot till the desired pH value (8 and 11).

Two different ZnO series have been obtained depending on the further thermal treatment applied. In the first case, the white precipitate was then filtered and washed with distilled water several times. This precursor was then dried overnight at 120 °C and further calcined at temperatures between 500 and 700 °C for 3 h.

For the second series, a certain volume of the white precipitate suspension obtained after TEA addition (150 ml, which corresponds to 75% of the total reactor volume) was placed in a Teflon recipient inside of stainless steel autoclave. The hydrothermal treatment was performed at 120 °C for 24 h. The precipitate was then filtered, repeatedly washed and dried overnight at 120 °C. Afterwards, thus obtained samples were submitted to a further calcination treatment. The influence of this thermal treatment was studied at temperatures similar to the previously described series.

BET surface area measurements were carried out by N₂ adsorption at 77 K using a Micromeritics 2000 instrument. Pore volumes were determined using the cumulative adsorption of nitrogen by the BJH method.

X-ray diffraction (XRD) patterns were obtained using a Siemens D-501 diffractometer with Ni filter and graphite monochromator. The X-ray source was Cu K α radiation (0.15406 nm). The line broadening (β_{hkl}) of X-ray diffraction peak corresponding to the (1 0 1), (0 0 2), (1 0 1), (1 0 2), (1 1 0), (1 0 3), (2 0 0), (1 1 2) and (2 0 1) planes was determined by deconvolution of the corresponding peak using a Voigt function. The amount of instrumental broadening was determined by using LaB₆ as a standard (NIST standard 660a). These values were incorporated into Williamson–Hall equation [15] for each sample according to the following expression:

$$\frac{\beta_{hkl} \cos \theta_{hkl}}{\lambda} = \frac{4\varepsilon \sin \theta_{hkl}}{\lambda} + \frac{1}{d}$$

where ε is the microstrain, d the crystallite size, λ the wavelength of the X-ray radiation 0.15406 nm and θ_{hkl} the diffracting angle.

Diffuse reflectance spectra were obtained on a UV–vis scanning spectrophotometer Varian Cary 100, equipped with an integrating sphere, using BaSO₄ as reference. UV–vis spectra were performed in the diffuse reflectance mode (R) and transformed to a magnitude proportional to the extinction coefficient (K) through the Kubelka–Munk function, $F(R_\infty)$. Band-gap values were obtained from the plot of the modified Kubelka–Munk function ($F(R_\infty) \times E$)^{1/2} versus the energy of the absorbed light E .

Scanning electron microscopy (SEM) pictures were taken on a JEOL JSM-5400 scanning electron microscope equipped with an energy dispersive X-rays analysis (EDX) link system for qualitative chemical analysis. Fractured samples were deposited on copper supports and covered by a thin film of gold.

Photocatalytic runs (2 h) of phenol oxidation over the different catalysts (1 g/l) were performed in a Pyrex immersion well reactor (450 ml) using a medium pressure 400 W Hg lamp supplied by Applied Photophysics, showing main emission line at 365 nm. In the oxidation tests, an oxygen flow was used to produce a homogenous suspension of the catalyst in the solution. Before each photo-experiment, the catalysts were settled in suspension with the reagent mixture for 15 min in the dark. The evolution of the initial phenol concentration (ca. 50 ppm in water) was followed by UV–vis spectrometry through the evolution of its characteristic 270 nm band, using a filtered aliquot ca. 2 ml of the suspension (Millipore Millex25 0.45 μ m membrane filter). Conversion rate values were obtained from the initial phenol degradation rate assuming zero order kinetic.

3. Results and discussion

3.1. Non-hydrothermally treated samples

In Table 1 we summarize the surface and structural features for samples obtained by calcination of filtered precipitate. It is worthy to note that the surface area values measured for this series are rather low. Even the uncalcined fresh precipitate exhibits significantly rather low surface area. Within this series, the pH of precipitation seems to affect considerably to the

Table 1
Surface and structural characterization for ZnO samples non-hydrothermally pre-treated

Temperature (°C)	pH 8				pH 11			
	S_{BET} (m ² /g)	Band-gap (eV)	d (nm)	$\varepsilon \times 10^3$	S_{BET} (m ² /g)	Band-gap (eV)	d (nm)	$\varepsilon \times 10^3$
120	44.4	3.2	19.3	1.3	15.3	3.2	39.0	6.8
500	9.6	3.2	49.6	1.2	6.5	3.2	56.4	1.4
600	5.0	3.2	48.2	1.1	4.9	3.2	46.2	0.8
700	3.7	3.2	82.8	1.0	1.6	3.2	82.8	1.1

surface area. And thus, at the lower pH, the surface area appears quite higher than at the highest pH. The further calcination treatment drastically reduces the surface values at both sets of samples.

All the diffraction patterns can be indexed to the hexagonal phase ZnO (Fig. 1). It is important to mention that even the fresh sample exhibits well-defined diffraction peaks corresponding to ZnO. In the case of pH 8 fresh sample additional small diffraction peaks associated to zinc acetate can also be observed. The calcination at different temperatures only induces narrower patterns, indicating a better crystallization in the system. By comparing the diffractograms for the two

pH sets of samples, it can be concluded that similar patterns are obtained except for the small variation in the peak relative intensities due to the differences in the crystalline growth conditions. Thus, in Fig. 2 we represent the relative intensity of peaks corresponding to the (1 0 0) and (0 0 2) planes taking as reference the intensity of (1 0 1) plane. Surprisingly, the evolution during calcination of the relative intensity for both peaks is completely different and depends on the precipitation pH. At the lower pH, the $I_{(0\ 0\ 2)}$ appreciably grows at calcination temperature increases while $I_{(1\ 0\ 0)}$ keeps the JCPDS reported relative intensity (JCPDS card no 36-1451). On the contrary, for the series obtained at pH 11, $I_{(1\ 0\ 0)}$ and $I_{(0\ 0\ 2)}$ decrease from the initial value for the fresh sample and follow an almost constant evolution with temperature, close to the reported values. This different progress with temperature clearly denotes a different crystallization growth, pointing out a clear preferential orientation in the case of sample prepared at pH 8.

From the Williamson–Hall plot we have calculated the size and microstrain contribution to the line broadening in the diffraction patterns (Table 1). The calculated crystallite sizes increase in similar way during calcination for both pH series. Size values develop in all cases from 20 to 40 nm to ca. 80 nm during calcination. There exists only a plain difference in the crystallite size for the fresh samples, being higher for the as-obtained sample at pH 11. The microstrain value (ε) also seems to be similar for both series, with values around 1.0×10^{-3} – 1.4×10^{-3} . This value is significantly lower than those reported by other authors [16], indicating a good crystallinity. Only in the case of the fresh sample obtained at pH 11, the microstrain appears significantly higher than all of the rest. This particular value is also in accordance with the lower surface area value as well as with the rather high value in the $I_{(0\ 0\ 2)}$ relative intensity. Therefore, it is clear that the as-obtained fresh sample at pH 11 might exhibit a particular structural feature clearly different than the corresponding fresh sample at pH 8.

In Fig. 3 we show the SEM micrographs corresponding to the non-hydrothermally treated set of samples. The fresh samples obtained exhibit clearly different morphologies (Fig. 3a and b). Thus, while the as-obtained sample at pH 8 show a laminar-like particles, fresh sample obtained at pH 11 presents spherical shape one of around 0.5 μm . This laminar disposition of sample at pH 8 would explain the results obtained from XRD patterns, in which a significantly higher value for $I_{(0\ 0\ 2)}$ is observed. Thus, a clear preferential orientation in the plane (0 0 2) might be associated with this morphology. After calcination at 700 °C (Fig. 3c and d) both samples present

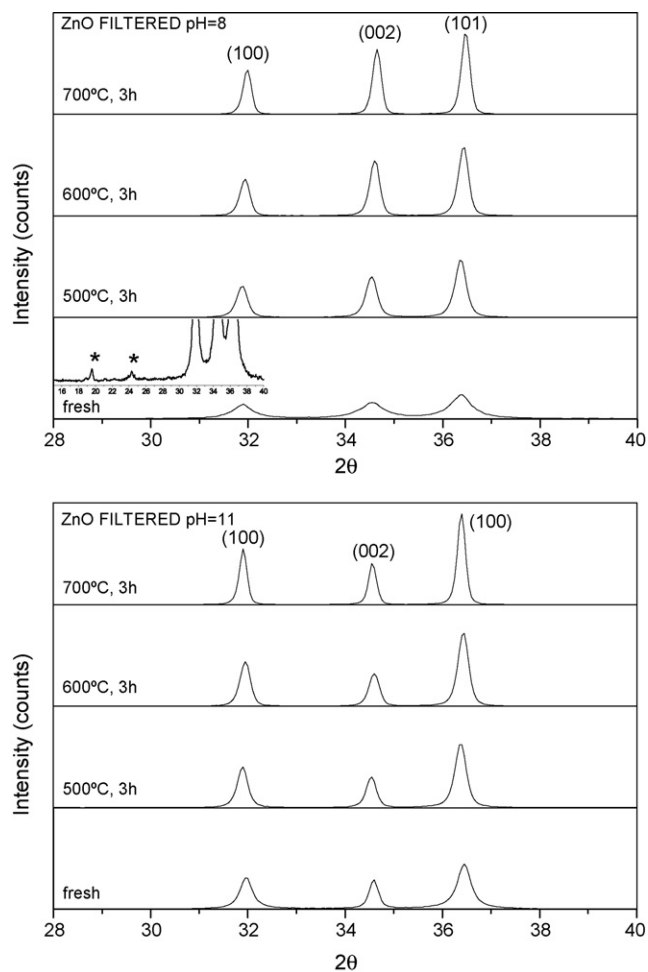


Fig. 1. XRD patterns corresponding to the non-hydrothermally pre-treated series calcined at different temperatures. Inset in the fresh sample plot shows peaks assigned to zinc acetate patterns.

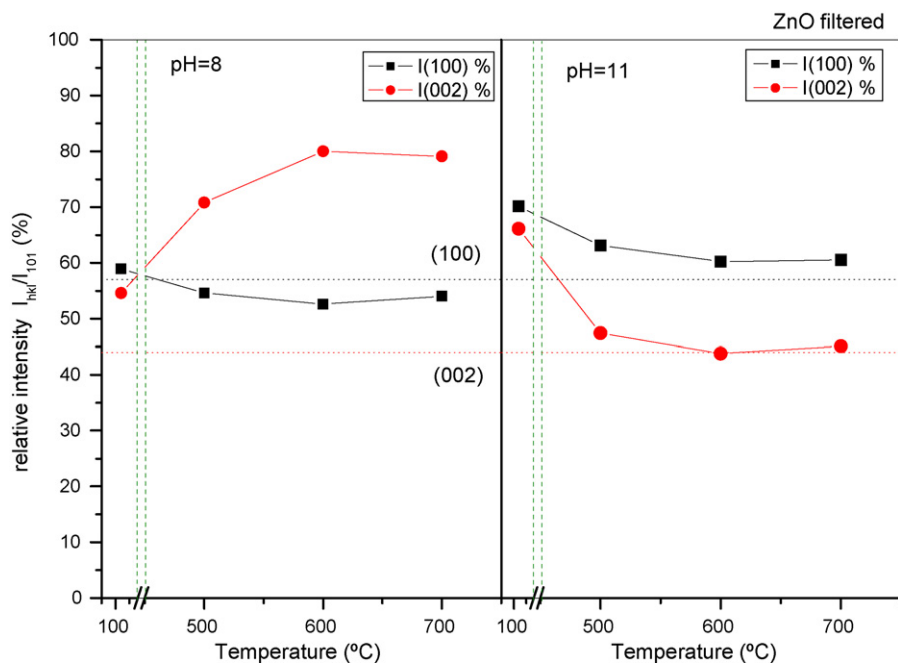


Fig. 2. Evolution during calcination of the I_{100} and I_{002} relative intensity for the non-hydrothermally pre-treated series.

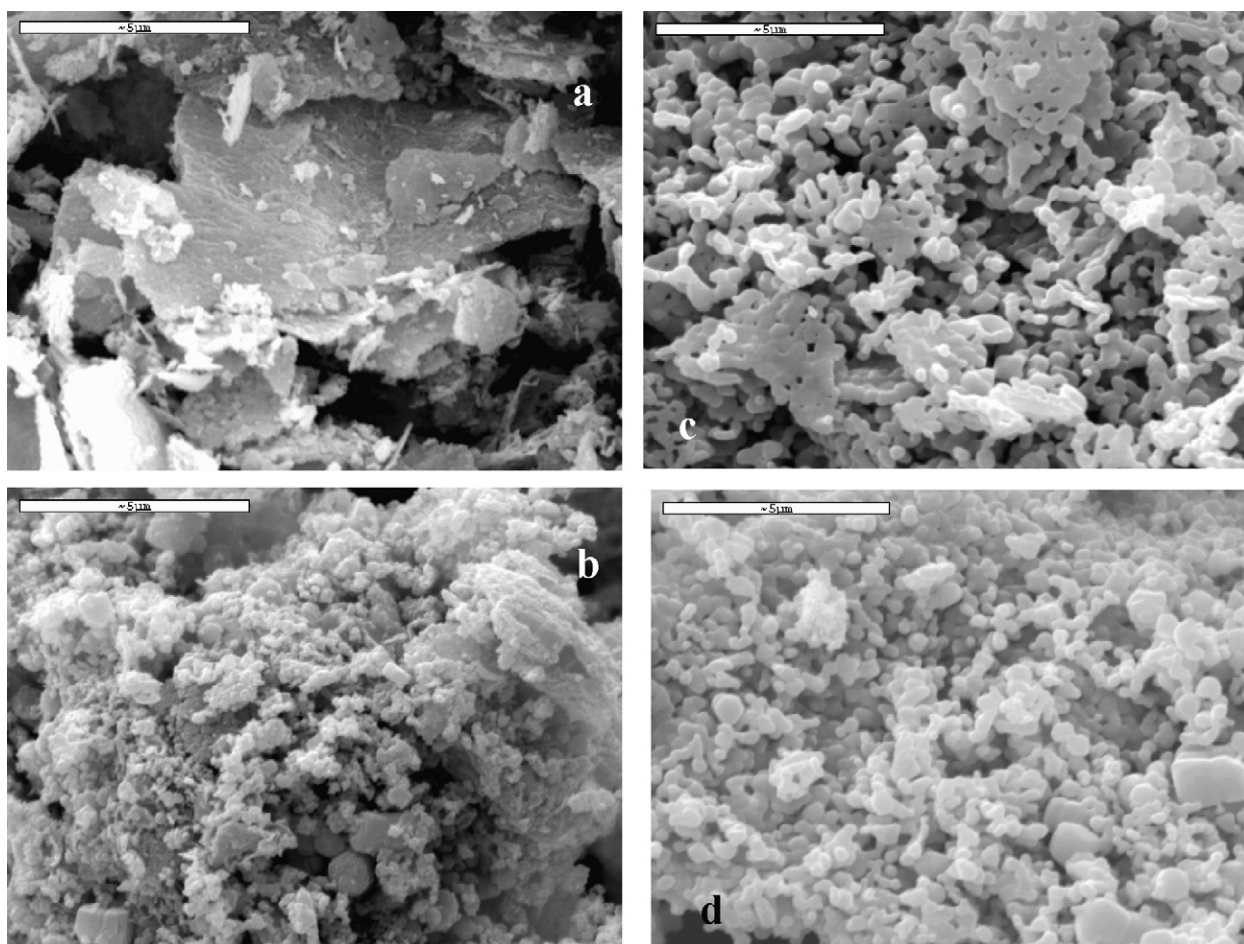


Fig. 3. Selected SEM images corresponding to the non-hydrothermally pre-treated (a) fresh as-prepared at pH 8, (b) fresh as-prepared at pH 11, (c) sample (a) calcined at 700 °C, 3 h, and (d) sample (b) calcined at 700 °C, 3 h.

homogeneous rounded particles. Moreover, in the case of the sample prepared at pH 8, these rounded particles are present in the form of somewhat planar aggregates reminding the original laminar particles.

Regarding to the optical absorption behaviour, all samples present similar absorption edge energies. Thus, the calculated band-gaps for all samples are around 3.2 eV.

The photoactivity test for these non-hydrothermally treated samples are shown in Fig. 4. From these results, it appears that catalysts prepared at the lower pH value exhibit slightly higher photoactivities, being in all cases higher than the photoactivity showed by the commercial Degussa P25 (dotted line in Fig. 4a). This difference between pH 8 and pH 11 series is more evident for the as-prepared ones. Probably, a less stable structure (notably high microstrain value) as well as the low surface area value (44 versus 15 m²/g) would be the responsible of this significantly lower reactivity. In addition, it seems that calcination treatment tends to diminish the reaction rates for both sets, especially for the series prepared at pH 11. Therefore, the best reaction rate is observed for uncalcined catalyst prepared at pH 8, while for pH 11 series the optimum values is observed for the catalysts calcined at 500 °C. By representing the reaction rate per surface area unit (Fig. 4b), we may infer

that the specific photoactivities are significantly higher in all cases with respect to Degussa P25. Furthermore, as calcination temperature increases the reaction rates follow an increasing progress for both series, denoting the improvement of the structure during calcination. Thus, it is worthy to note that these systems remarkably enhance their photocatalytic activity upon calcination. Though the specific surface areas for calcined ZnO are notably low after calcination at 700 °C, the photoactivity values do not decrease as drastically as surface. Then, as reaction rates for these samples keep very acceptable values, the specific reaction rates grow exponentially. Within these systems the structural features contribution to the photoactivity is undoubtedly more critical as the surface one.

3.2. Hydrothermally treated samples

In order to improve the photoactivity of ZnO systems, we have performed a hydrothermal treatment previous to the thermal annealing. In Table 2 we summarize these sets of systems. The first point that surprises is that the hydrotreatment drastically suppresses the surface area values. Both systems, before calcination, show particularly low surface area around 1.5 m²/g. The further calcination vaguely affect to the initial surface area values, which remain in all cases around 1 m²/g, largely different from those reported for ZnO obtained by hydrothermal treatment [17,18].

Regarding the crystalline evolution of these series, all patterns can be ascribed to the wurtzite ZnO phase (Fig. 5). From the analysis of the peak relative intensity corresponding to (1 0 0) and (0 0 2) planes, we may infer a plain different structural situation from the non-hydrothermally treated series. Thus, for hydrotreated systems, both pH sets of samples show an apparent preferential growth in the (0 0 1) direction (Fig. 6), leading to important $I_{1\ 0\ 0}$ values. Even in the case of the sample calcined at 700 °C from the pH 8 series the peak corresponding to the (1 0 0) plane becomes the most intense peak. This behaviour is plainly different from that observed in the previous series, indicating that hydrothermal treatment induces a different crystallization growth along the (0 0 1) direction. In fact, zinc and oxygen atoms are arranged alternatively along the *c*-axis. Therefore, and as it well established, this inherent asymmetry along the *c*-axis results in the anisotropic growth of ZnO crystallites.

The crystallite sizes calculated from the Williamson–Hall equation appear almost constant within each pH series during calcination. In addition, it can be seen that for pH 8 series the crystallite size appear to be relatively higher than those calculated for the pH 11 series. Thus, while samples obtained at pH 8 exhibit an average size of 85 nm, those obtained at pH 11 present ca. 75 nm. The estimated microstrain values also become slightly lower for the pH 8 series, confirming the best crystallinity of this series. For pH 11 series the strain values are in all cases above 1.2×10^{-3} , while for the pH 8 series these values are located around 1.0×10^{-3} .

The morphology of these hydrotreated systems is shown in Fig. 7. As in the previous case, the SEM images of these samples present a certain relationship between the morphology

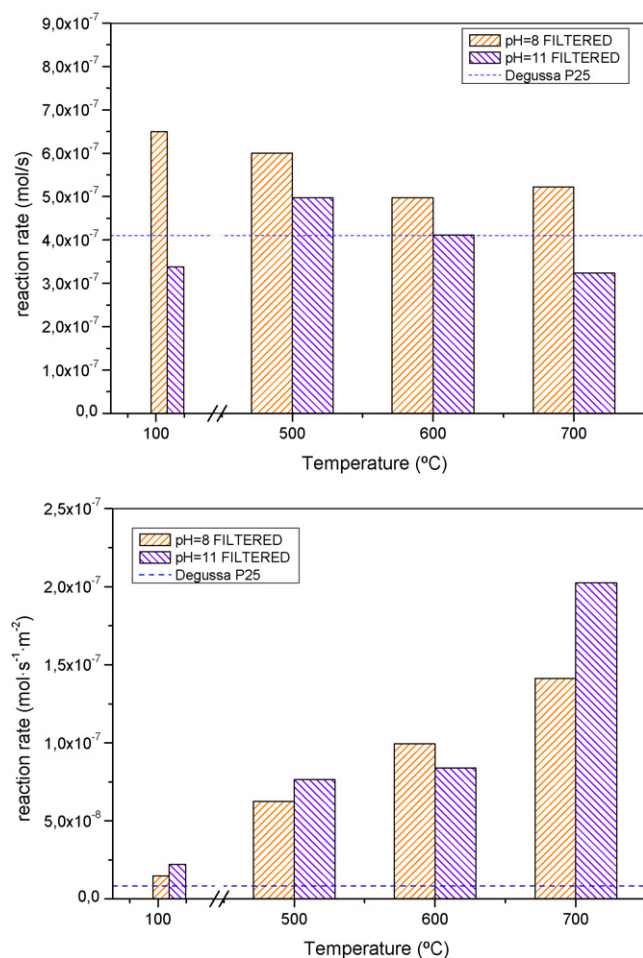


Fig. 4. (a) Photocatalytic activity of the non-hydrothermally obtained systems. (b) Photocatalytic activity per surface area unit of the non-hydrothermally obtained systems.

Table 2
Surface and structural characterization for ZnO samples hydrothermally pre-treated

Temperature (°C)	pH 8				pH 11			
	S_{BET} (m ² /g)	Band-gap (eV)	d (nm)	$\varepsilon \times 10^3$	S_{BET} (m ² /g)	Band-gap (eV)	d (nm)	$\varepsilon \times 10^3$
120 (HT)	1.0	3.2	91.2	0.8	1.5	3.2	85.1	1.2
500	1.0	3.2	93.5	1.2	1.0	3.2	67.8	1.3
600	1.2	3.2	80.6	0.7	1.0	3.2	79.7	1.5
700	1.5	3.2	80.5	1.1	1.5	3.2	71.9	1.4

and the preparation pH. Thus, samples prepared at pH 8 exhibit well-developed hexagonal prism-like particles. The formation of hexagonal prism shaped ZnO crystals in the present study is suggested to be attributed to the difference in the growth rate of the various crystal facets [19,20]. From these considerations, the shape of ZnO structures will be determined by the relative growth of these different crystal faces influenced by the type of thermal treatment (thermal or hydrothermal) as well as the presence of TEA used for the precipitation, that could also act as capping agent.

On the contrary, samples precipitated at pH 11 show rice-like particles, forming in some cases flower-like assemblies. Both geometrical shapes would explain the preferential orientation

observed in the XRD patterns, in which the peak corresponding to the (1 0 0) plane markedly emerges. As it was stated, pH 8 series present I_{100} relative intensities slightly higher than those calculated for pH 11. This slight difference would be related to the difference between prismatic and rice-like shapes in each case. Regarding to this, it has been reported that the relative amount of $\text{Zn}(\text{OH})_2$ precipitate and $[\text{Zn}(\text{NH}_3)_4]^{2+}$ species in the precursor solution will determine the anisotropic growth of ZnO when the pH value is larger than 7 [21,22]. Thus, in our case TEA would also act as capping agent, which may control and direct the final morphology depending on the precipitation pH [23]. The further calcination treatment does not change the initial morphology.

The photocatalytic activity of hydrothermal pre-treated systems is reported in Fig. 8. In principle, the photoactivities observed for this series become improved with the further calcination treatment (Fig. 8a). Thus, samples calcined at 600 and 700 °C exhibit larger reaction rates values. Within the pH 8 series the best photocatalytic behaviour is reached after calcination at 600 °C, while for pH 11 series the best value is observed at 700 °C. These optimum reaction rates values are better than the best values obtained for the non-hydrothermally pre-treated series (Fig. 4a), and even much better than the reaction rate for Degussa P25. In this sense, Li et al. reported the interesting correlations between structural features of ZnO and the final photocatalytic activity [24]. Thus, higher relative I_{100}/I_{002} ratio seems to enhance the ZnO photoactivity for acetaldehyde decomposition. In our case, hydrothermally obtained systems present important preferential orientation in the (0 0 1) direction, not observed in the non-hydrothermally treated samples. This fact implies that hydrothermally treated series will show particles highly exposed in the (1 0 0) face, described as the most photoactive one by Li et al. [24]. In fact, the (1 0 0) face for ZnO hexagonal structure is considered the most stable one and additionally with a clear non-polar character [25]. This important fact would also contribute and affect to the photocatalytic properties in any way.

Moreover, and considering the extremely low surface area value of these hydrothermally pre-treated series (Table 2), it is obvious that the specific reaction rates values per surface area unit will be higher than those observed for non-hydrothermally pre-treated series. In Fig. 8b we show the evolution of the specific rates of reaction for these systems. It is worthy to note the markedly difference of these values with respect to previous series as well as to Degussa P25. It can be pointed out that the good structural features of these ZnO systems strongly affect to their final photocatalytic activity. Since the surface area values

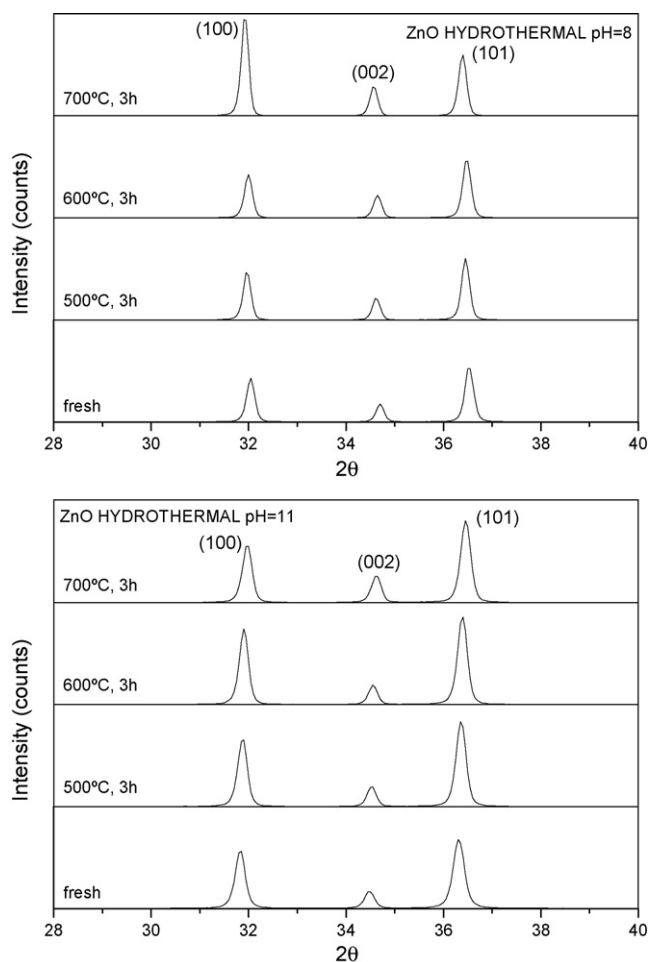


Fig. 5. XRD patterns corresponding to the hydrothermally pre-treated series calcined at different temperatures.

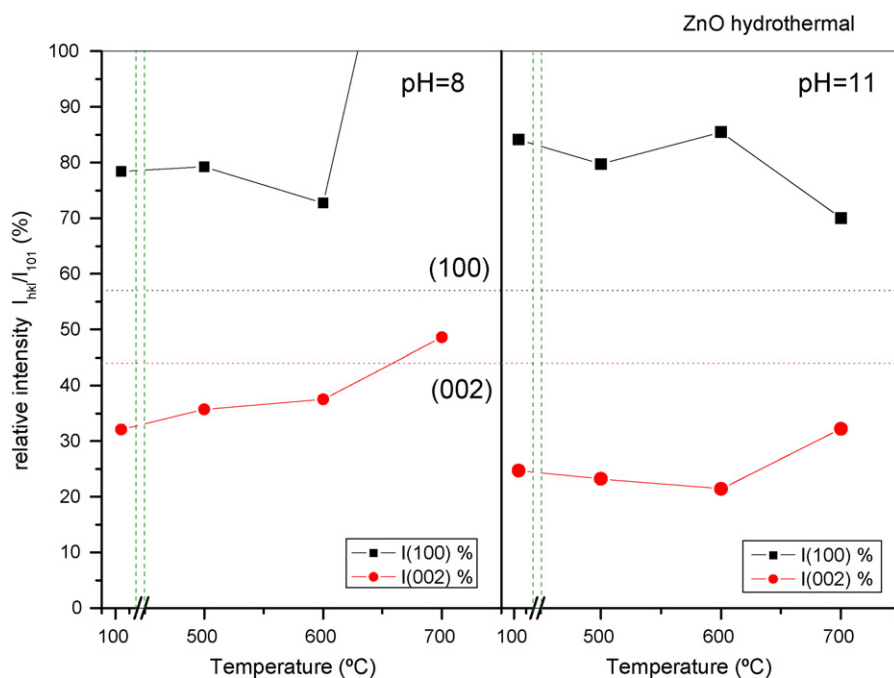


Fig. 6. Evolution during calcination of the I_{100} and I_{002} relative intensity for the hydrothermally pre-treated series.

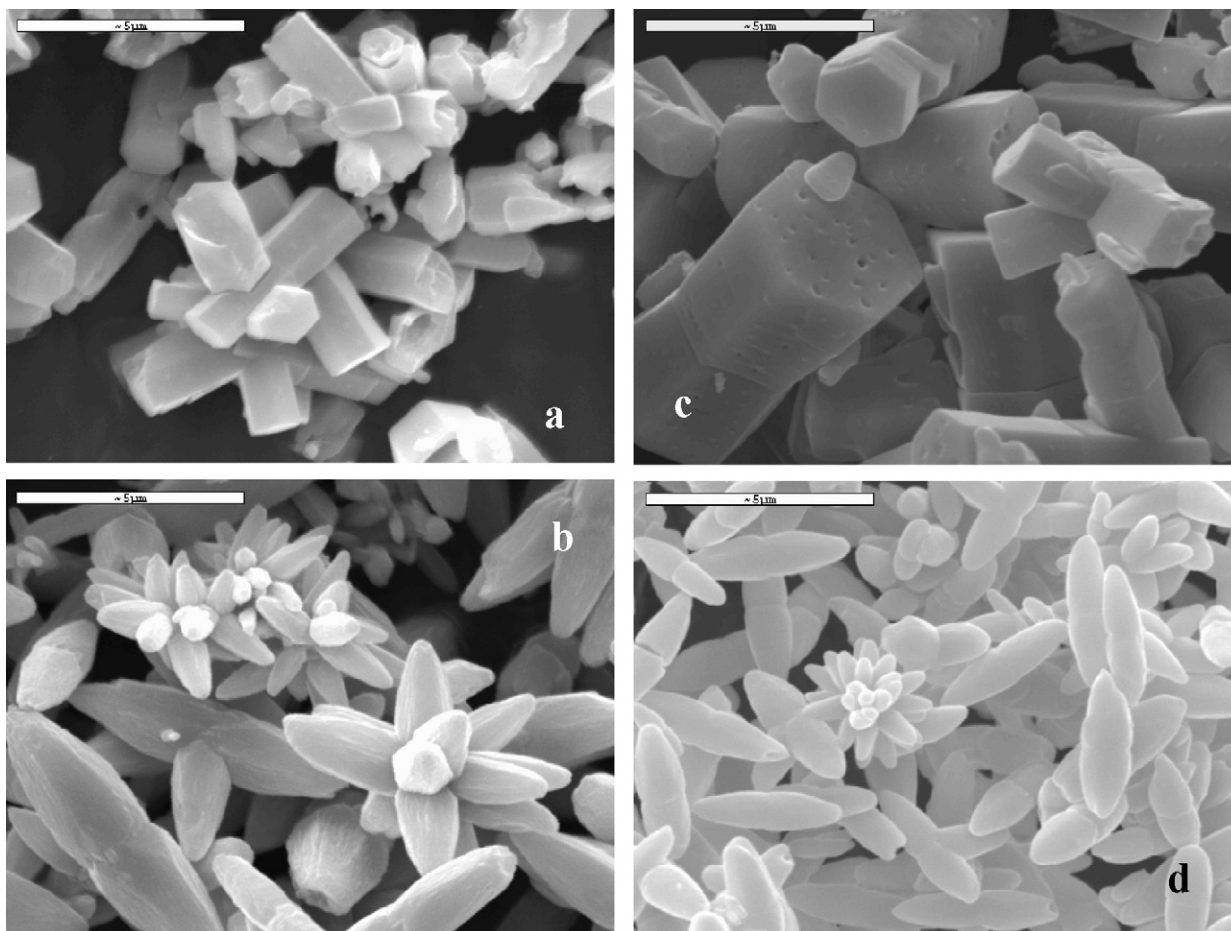


Fig. 7. Selected SEM images corresponding to the hydrothermally pre-treated (a) fresh as-prepared at pH 8, (b) fresh as-prepared at pH 11, (c) sample (a) calcined at 700 °C, 3 h, and (d) sample (b) calcined at 700 °C, 3 h.

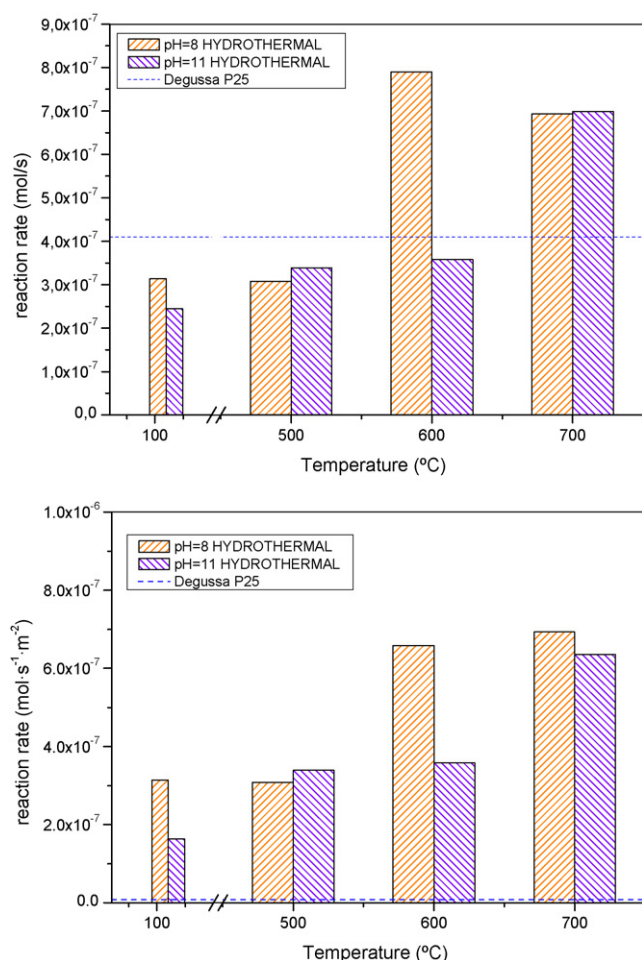


Fig. 8. (a) Photocatalytic activity of the hydrothermally obtained systems. (b) Photocatalytic activity per surface area unit of the hydrothermally obtained systems.

are extremely low, the specific photocatalytic activity comes out fairly good. Therefore, we might conclude that the hydrothermal pre-treatment leads to excellent structural situation for the electronic processes involved in the photocatalytic mechanism.

4. Conclusions

We have prepared ZnO systems from aqueous Zn²⁺ solution and further precipitation with TEA at two different pH values. The solid obtained directly from the filtration of these precipitates exhibits hexagonal wurtzite structure (space group P6₃mc). After calcination at different temperature a certain sintering process takes place and surface area progressively diminishes and crystallite size increases. The microstrain values indicate that calcination clearly reduces the crystalline defects in the structure similarly in both pH series. The major difference appear in the morphology observed for these series, leading to clear preferential orientation in the case of pH 8 series. The photocatalytic activities of these sets of samples follow a slight decrease as temperature increases, probably due to the surface area diminution. However, the specific reaction rates clearly indicate that the enhancement in the structural

features affects in a greater way than surface area. Within the two pH series, the best behaviour is found for the samples calcined at 700 °C, being notably higher than the value observed for Degussa P25.

We have also studied the influence of hydrothermal pre-treatment before the calcination. The corresponding series also exhibit well-crystallized ZnO structure before the calcination. Such treatment leads to a better structural situation and at the same time to the suppression of surface area. In spite of this, the photocatalytic behaviour of these systems appears surprisingly high. Furthermore, as pH increases the optimum calcination temperatures shifted from 600 to 700 °C, respectively. The structural excellence of such systems clearly enhances their photoactivity values. Thus, the specific rates of reaction are manifestly superior with respect to the non-hydrothermally pre-treated series as well as Degussa P25. The precipitation by means of TEA clearly affects to the final structural features, morphology and surface. The capping-assisted hydrothermal preparation of ZnO leads to the conjunction of mentioned factors, leading to a highly photoactive system.

Acknowledgements

Financial support (projects CTQ2004-05734-C02-01 and CTQ2004-05734-C02-02) and Junta de Andalucía (P.A.I. group references FQM181 and project P06-FQM-1406) are acknowledged. Ms. E. Pulido also wanted to thank her exchange fellowship within the FPI programme by the Spanish Ministerio de Educación y Ciencia.

References

- [1] G. Colón, C. Beller, M. Fernández-García, Nanostructured oxides in photocatalysis, in: *Synthesis, Properties and Application of Oxide Nanoparticles*, M. Fernández-García, J.A. Rodríguez (Eds.) Wiley, USA, 2007 (Chapter 17) (ISBN: 978-0-471-72405-6).
- [2] O. Carp, C.L. Huisman, A. Reller, *Prog. Solid State Chem.* 32 (2004) 33.
- [3] H. Yumoto, T. Inoue, S.J. Li, T. Sako, K. Nishiyama, *Thin Solid Films* 345 (1999) 38.
- [4] E. Vasco, O. Böhme, E. Román, *J. Phys. Chem. C* 111 (2007) 3505.
- [5] B.-Z. Fang, G.-J. Dong, J.-F. Wang, W.-J. Guan, X.-Z. Zhao, *J. Appl. Phys.* 101 (2007) 033713.
- [6] J.C. Johnson, H. Yan, R.D. Schaller, L.H. Haber, R.J. Saykally, P. Yang, *J. Phys. Chem. B* 105 (2001) 11387.
- [7] U. Alver, T. Kılınc, E. Bacaksız, T. Küçükömeroğlu, S. Nezir, İ.H. Mutlu, F. Aslan, *Thin Solid Films* 515 (2007) 3448.
- [8] P. Yang, H. Yan, S. Mao, R. Russo, J. Johnson, R. Saykally, N. Morris, J. Pham, R. He, H.-J. Choi, *Adv. Funct. Mater.* 12 (2002) 323.
- [9] H. Van den Rul, D. Mondelaers, M.K. Van Bael, J. Mullens, *J. Sol–Gel Sci. Technol.* 39 (2006) 41.
- [10] U. Pal, P. Santiago, *J. Phys. Chem. B* 109 (2005) 15317.
- [11] F. Xu, Z.-Y. Yuan, G.-H. Du, M. Halasa, B.-L. Su, *Appl. Phys. A* 86 (2007) 181.
- [12] Y.V. Kolen'ko, B.R. Churagulov, M. JKunst, L. Mazerolles, C. Colbeau-Justin, *Appl. Catal. B: Environ.* 54 (2004) 51.
- [13] M.C. Hidalgo, M. Aguilar, M. Maicu, J.A. Navío, G. Colón, *Catal. Today* 129 (2007) 50.
- [14] G. Colón, M.C. Hidalgo, J.A. Navío, E. Pulido Melían, O. González Díaz, J.M. Doña Rodríguez, *Appl. Catal. B: Environ.* 78 (2008) 176.
- [15] G.K. Williamson, W.H. Hall, *Acta Metall.* 1 (1953) 22.
- [16] L.P. Bauermann, J. Bill, F. Aldinger, *J. Phys. Chem. B* 110 (2006) 5182.

- [17] A.S. Shaporev, V.K. Ivanov, A.E. Baranchikov, Y.D. Tret'yakov, *Inorg. Mat.* 43 (2007) 35.
- [18] J. Liang, S. Bai, Y. Zhang, M. Li, W. Yu, Y. Qian, *J. Phys. Chem. C* 111 (2007) 1113.
- [19] R.A. Laudies, A.A. Ballman, *J. Phys. Chem.* 64 (1960) 688.
- [20] J. Zhang, L. Sun, J. Yin, H. Su, C. Liao, C. Yan, *Chem. Mater.* 14 (2002) 4172.
- [21] H. Zang, D. Yang, Y. Ji, X. Ma, J. Xu, D. Que, *J. Phys. Chem. B* 108 (2004) 3955.
- [22] H. Zang, D. Yang, X. Ma, Y. Ji, J. Xu, D. Que, *Nanotechnology* 15 (2004) 622.
- [23] H. Zhang, D. Yang, D. Li, X. Ma, S. Li, D. Que, *Cryst. Growth Des.* 5 (2005) 547.
- [24] D. Li, V. Balek, N. Ohashi, T. Mitsuhashi, S. Hishita, H. Haneda, *J. Colloid Interface Sci.* 289 (2005) 472.
- [25] L. Vayssieres, K. Keis, A. Hagfeldt, S.E. Lindquist, *Chem. Mater.* 13 (2001) 4395.